LETTERS
PUBLISHED ONLINE: 23 FEBRUARY 2015 | DOI: 10.1038/NPHYS3240
nature physics

Direct observation of Josephson vortex cores

Dimitri Roditchev[1,2], Christophe Brun[1], Lise Serrier-Garcia[1], Juan Carlos Cuevas[3], Vagner Henrique Loiola Bessa[4], Milorad Vlado Milošević[4,5], François Debontridder[1], Vasily Stolyarov[1] and Tristan Cren[1]*

Superconducting correlations may propagate between two superconductors separated by a tiny insulating or metallic barrier, allowing a dissipationless electric current to flow[1,2]. In the presence of a magnetic field, the maximum supercurrent oscillates[3] and each oscillation corresponding to the entry of one Josephson vortex into the barrier[4]. Josephson vortices are conceptual blocks of advanced quantum devices such as coherent terahertz generators[5] or qubits for quantum computing[6], in which on-demand generation and control is crucial. Here, we map superconducting correlations inside proximity Josephson junctions[7] using scanning tunnelling microscopy. Unexpectedly, we find that such Josephson vortices have real cores, in which the proximity gap is locally suppressed and the normal state recovered. By following the Josephson vortex formation and evolution we demonstrate that they originate from quantum interference of Andreev quasiparticles[8], and that the phase portraits of the two superconducting quantum condensates at edges of the junction decide their generation, shape, spatial extent and arrangement. Our observation opens a pathway towards the generation and control of Josephson vortices by applying supercurrents through the superconducting leads of the junctions, that is, by purely electrical means without any need for a magnetic field, which is a crucial step towards high-density on-chip integration of superconducting quantum devices.

In 1963 Rowell[3] observed the oscillations of the critical current in superconducting junctions subject to a magnetic field. Since his pioneering discovery, the effect has been reported in numerous superconductor–normal metal–superconductor (SNS) weak links[4,9], including many examples in which the links were made of recently discovered materials such as graphene[10] and topological insulators[11,12]. This macroscopic quantum interference effect is commonly interpreted as a sequence of Josephson vortices[4] penetrating the junction. By analogy with the Abrikosov vortices in type II superconductors[13], Josephson vortices were defined as regions with zero net circulating current and enclosing a magnetic flux quantum, $\Phi_0 = h/2e$. Several theoretical works, motivated by superconducting vortex pinning at grain boundaries[14–18], studied the large-scale evolution of Abrikosov[18] and Pearl[19,20] vortices in the S-parts of zero-width tunnel junctions. Yet, the spectral fingerprint of Josephson vortices and their spatial organization in the N-parts of extended Josephson junctions have so far remained undecided, and the subject of controversy. The common wisdom is that Josephson vortices lack a specific spectral signature and therefore cannot be identified. By contrast, recent microscopic calculations predicted that in diffusive SNS junctions Josephson vortices should be manifested as a spatial modulation of the proximity mini-gap in the quasiparticle excitation spectrum of the normal region of the junction[7]. Thus, Josephson vortices could presumably have normal cores—regions where the proximity gap vanishes, making possible their detection and imaging by, for example, scanning tunnelling microscopy (STM), as is readily done for Abrikosov vortices in superconductors[21].

With this idea in mind, we created (see Methods) a lateral SNS network of superconducting Pb nanocrystals (yellow areas in Fig. 1a) linked together by an atomically thin Pb wetting layer (brown regions in Fig. 1a). Depending on the growth conditions, the Pb wetting layer is superconducting when it is crystalline[16,22], whereas it is metallic when its structure is amorphous[23]. The Pb islands become superconducting below a critical temperature $T_c \approx 6.5\,\mathrm{K}$ (refs 24–28). The local tunnelling conductance spectra measured on top of the superconducting islands at $T = 0.3\,\mathrm{K} \ll T_c$ (see Methods) exhibit a superconducting gap $\Delta = 1.2\,\mathrm{meV}$ (Fig. 1d, curve S). Here, the wetting layer is non-superconducting, and the conductance spectra measured far from the islands show no superconducting gap, but rather a tiny dip centred at the Fermi level (Fig. 1d, curve WL). This dip is a fingerprint of the Altshuler–Aronov zero-bias anomaly[29] due to electron–electron interaction in this two-dimensional diffusive metal[23]. Very close to the islands the superconducting correlations induce a small proximity gap in tunnelling spectra of the wetting layer[23] (Fig. 1d, curve P). In the zero-bias conductance map in Fig. 1b the proximity gap appears as a bluish halo extending over a few tens of nanometres away from islands. In locations where the edges of neighbouring islands get very close, this proximity halo becomes reinforced and appears as a deeper blue. The phenomenon reflects the overlap of superconducting correlations induced by both islands[30–32], which enhance the proximity gap (Fig. 1d, curve J). This results in the formation of several SNS Josephson junctions, such as those seen in locations J1–J4 (Fig. 1b,c).

We now follow the evolution of the proximity links in an applied magnetic field. The spectroscopic map acquired at 60 mT shows the usual penetration of Abrikosov vortices in the large islands, whereas the small islands remain in the vortex-free Meissner state[28] (Fig. 1c). By contrast, unusual features are revealed in proximity links inside the SNS junctions, and identified as Josephson vortices. Precisely, whereas at zero field the proximity gap is observed in all three locations A, B, C of the junction J1 (see Fig. 1b and zoom of J1 in Fig. 1e), at 60 mT no proximity gap is observed in B (red spectrum in Fig. 1f), but instead a normal state with its Altshuler–Aronov zero-bias dip is recovered. In the neighbouring positions A and C, however, the proximity gap persists (Fig. 1e,f). This behaviour

[1]Institut des Nanosciences de Paris, Sorbonne Universités, UPMC Univ Paris 6 and CNRS-UMR 7588, F-75005 Paris, France. [2]Laboratoire de Physique et d'Etude des Matériaux, ESPCI-ParisTech, CNRS and UPMC Univ Paris 6 - UMR 8213, 10 rue Vauquelin, 75005 Paris, France. [3]Departamento de Física Teórica de la Materia Condensada and Condensed Matter Physics Center (IFIMAC), Universidad Autónoma de Madrid, 28049 Madrid, Spain. [4]Departamento de Física, Universidade Federal do Ceará, 60451-970 Fortaleza, Ceará, Brazil. [5]Departement Fysica, Universiteit Antwerpen, Groenenborgerlaan 171, B-2020 Antwerpen, Belgium. *e-mail: tristan.cren@upmc.fr

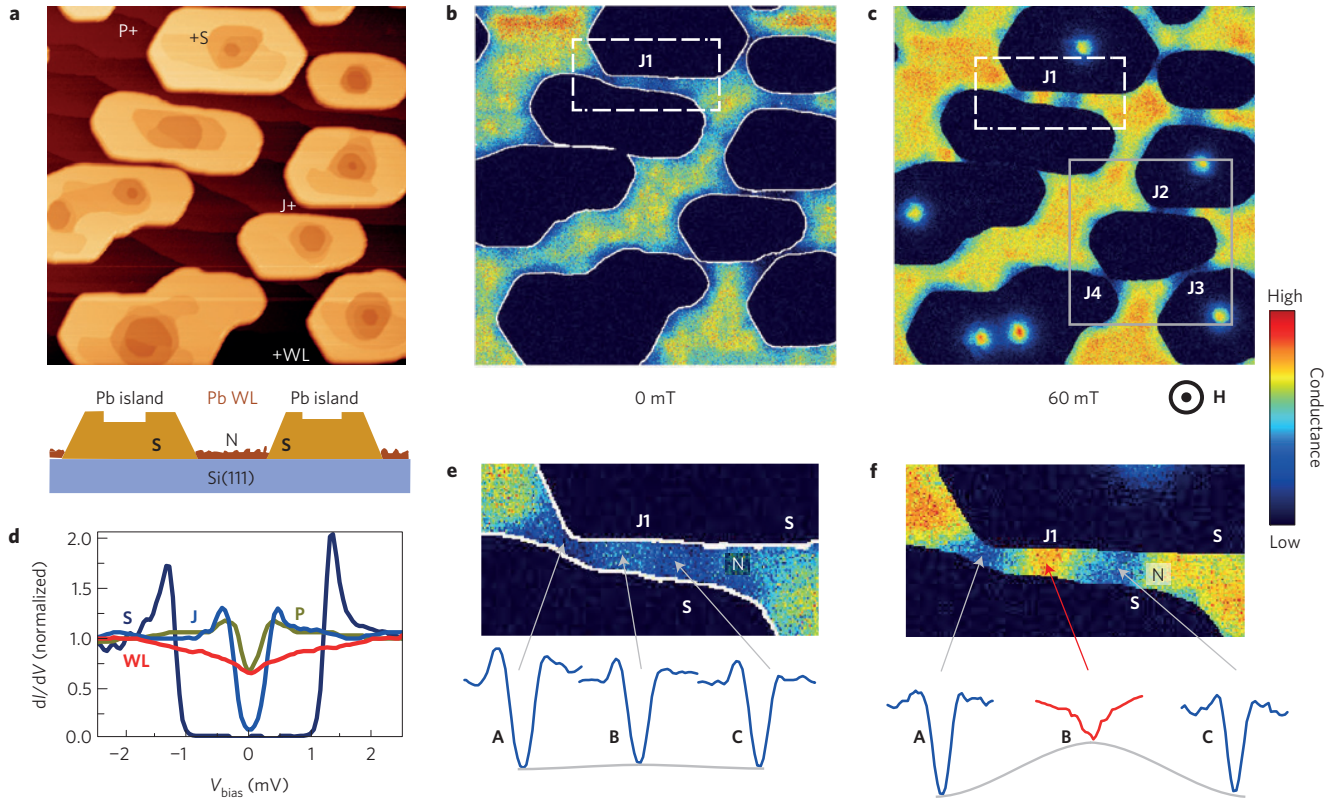

Figure 1 | Josephson vortices imaged by scanning tunnelling spectroscopy at 0.3 K. a, Topographic STM image of a 1,000 nm × 1,000 nm area of the sample. 12–14 monolayer-thick Pb islands are yellow. They are surrounded by an atomically thin two-dimensional disordered metal, the Pb wetting layer, which is brown. The bottom panel gives a schematic cross-sectional view of the sample. Superconducting–normal–superconducting (SNS) proximity junctions are formed between the closest edges of adjacent Pb islands through the wetting layer region situated between the island edges. **b**,**c**, Colour-coded tunnelling conductance maps $dI(V)/dV(X,Y)$ at zero-bias $V=0$ V of the same sample area, acquired in zero field (**b**) and a perpendicular magnetic field of 60 mT (**c**). In zero field (**b**), the SNS junction J1 (inside the dashed white box) shows a rather homogeneous proximity effect, emphasized by a low-conductance region (deep blue). However at 60 mT (**c**) a single Josephson vortex appears inside the proximity area of J1 as a bright yellow spot surrounded by two blue superconducting Josephson links. **d**, Characteristic local tunnelling conductance spectra measured at the locations indicated in **a**: superconducting Pb islands (curve S), non-superconducting wetting layer far from islands (curve WL), wetting layer in the proximity region (curve P), and wetting layer inside a proximity SNS junction (curve J). **e**,**f**, Zoom of the J1 SNS proximity junction together with corresponding tunnelling spectra at three locations A, B, C in J1, at zero field (**e**) and in a magnetic field of 60 mT (**f**). As a Josephson vortex sets in, the proximity gap in its core vanishes (red curve B in **f**). Three other junctions denoted J2, J3 and J4 in the bottom framed region are further studied in Fig. 2.

is confirmed by the direct inspection of the conductance map in Fig. 1f, where two clear Josephson links remain at 60 mT in locations A and C (low conductance in blue), whereas in B the proximity gap vanishes (high conductance in yellow-red). The normal region in B surrounded by gapped areas is thus indeed a Josephson vortex core. The spectroscopic maps in Fig. 2a,b focus on junctions J2, J3 and J4, located in the bottom framed part of Fig. 1c. They show how Josephson vortex configurations change with magnetic field. Both J2 and J3 junctions accept one Josephson vortex at 120 mT (Fig. 2a) and two at 180 mT (Fig. 2b). A striking effect is observed inside the junction J2. At 120 mT the proximity gap is destroyed in its centre, where a Josephson vortex core settles (Fig. 2a). At 180 mT, however, this region returns to the proximity gapped state, thus separating two neighbouring Josephson vortex cores (Fig. 2b). By contrast, the very short and narrow junction J4 does not accept any Josephson vortex in its centre up to 180 mT. In all studied SNS junctions, Josephson vortex cores are in the normal state, as predicted[7].

The interpretation of our observation in terms of Josephson vortex cores is fully corroborated by the numerical simulations in Fig. 2c,d; the calculation method is described in Fig. 3. We first calculated the Abrikosov vortex configurations in the islands using the Ginzburg–Landau formalism (Supplementary Information 1). As an example, in Fig. 3a the Cooper-pair density map calculated at 60 mT reproduces the experimentally observed Abrikosov vortex configuration (Fig. 1c). In Fig. 3b the corresponding phase portrait of the superconducting order parameter shows that the interplay between Meissner and vortex currents results in a spatially evolving phase inside islands. At this point, the physical origin of Josephson vortices can be understood by considering the gauge-invariant local phase difference across the junction, $\varphi^*=\varphi(r_2)-\varphi(r_1)-(2e/\hbar)\int_{r_1}^{r_2}\mathbf{A}\mathrm{d}\mathbf{l}$, where $\varphi(r_i)$ are local phases of the order parameter at two island edges at positions r_i (on opposite sides of a given junction) and $\mathbf{A}$ is the vector potential (Supplementary Information 2). At locations in which φ^* is 0, $\pm2\pi, \pm4\pi, \pm6\pi, \ldots$, the superconducting correlations induced by both islands are in phase, their constructive interference resulting in a well-developed proximity gap. In contrast, in locations where φ^* is $\pm\pi, \pm3\pi, \pm5\pi \ldots$ the superconducting correlations interfere destructively and the proximity gap is suppressed[33]. This latter situation corresponds to Josephson vortex cores. Using φ^* we find a current circulating around Josephson vortices. As a rough approximation, the Josephson current[2] can be considered locally as simply proportional to $\sin(\varphi^*)$. In junction J1, for instance, in locations between A and B, φ^* varies continuously from 0 to π, $\sin(\varphi^*)>0$ and some net Josephson current flows locally from one island edge to the other island. In the opposite case, from B to C the

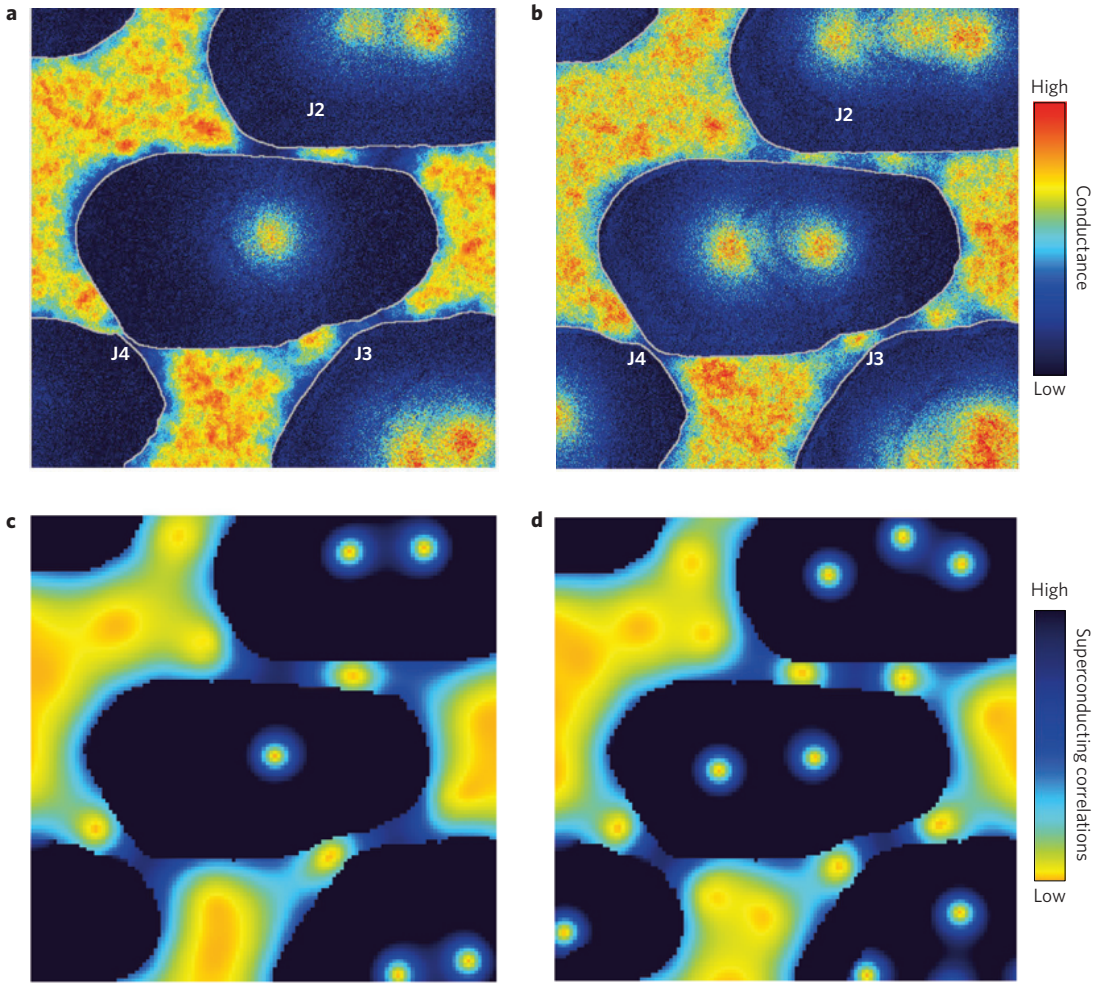

Figure 2 | Josephson vortex formation and evolution with magnetic field. a, Colour-coded zero-bias tunnelling conductance map of the selected region, 400 nm × 400 nm (indicated in Fig. 1c), showing Josephson vortex formation in three SNS junctions (denoted J2, J3 and J4) at 120 mT. Josephson vortex cores are detected in the normal part of the junctions J2 and J3 as high-conductance regions indicated by bright yellow spots (locally destroyed mini-gap) surrounded by low-conductance regions (blue). The shortest junction J4 contains no Josephson vortices. **b**, Conductance map of the same area at 180 mT. The comparison between maps **a** and **b** evidences the evolution of Josephson vortices with magnetic field. **c**,**d**, Correlation maps at 120 mT and 180 mT show the Josephson vortices more clearly. The maps were numerically generated on the basis of the suggested self-consistent gauge-invariant model (see Fig. 3 and explanations in the text). Note that the simulation perfectly reproduces the number, spatial extent and position of Josephson vortices inside the junctions.

phase difference φ^* varies continuously from π to 2π, $\sin(\varphi^*) < 0$, and the current flows in the opposite direction. Therefore, Josephson current circulates around the point B, thus justifying the term 'Josephson vortex'. The above phase considerations served as a basis for numerical simulations. First, the superconducting phase portrait $\varphi_{GL}(\mathbf{r})$ was generated using Ginzburg–Landau formalism for independent islands. This phase portrait is not unique: it varies depending on the choice of the gauge. Figure 3b shows one of such phase portraits obtained using the symmetric gauge $\mathbf{A}(\mathbf{r}) = (1/2)\mathbf{B} \times \mathbf{r}$, where $\mathbf{B}$ is the magnetic field, with the origin in the image centre. Because islands are decoupled, the phase portrait is defined up to arbitrary constant phases α_i for each ith island (that is, one can freely use $\varphi(\mathbf{r}_i) = \varphi_{GL}(\mathbf{r}_i) + \alpha_i$, without affecting the superconducting state in the islands). Once the islands are proximity-coupled, the difference $\alpha_i - \alpha_j$ between two island phases of the same junction is no longer arbitrary but respects two constraints: first, in the absence of an external circuit the total Josephson current crossing a junction is null; second, the free energy of the Josephson junctions is minimized. Starting from the phase portrait in Fig. 3b, we calculated, for each location inside the junctions, the strength of the superconducting correlations as the interference between evanescent waves having a gauge-independent phase difference $\varphi^*(\mathbf{r})$. In these calculations we fulfilled the above constraints and fixed the island phases α_i self-consistently, with no need for adjustable parameters (for more details see Supplementary Information 2). The result of our calculations is shown in Fig. 3c, ideally reproducing the experimentally observed position and extent of the Josephson vortex in the junction J1 (Fig. 1c). In the same manner the correlation maps in Fig. 2c,d were calculated, again matching the experimental findings (Fig. 2a,b). The success of our simulation clearly highlights that the Josephson vortices in our system originate from quantum interference.

Next, we calculated the spatial evolution of the density of states inside the Josephson vortex core, which cannot be obtained from correlation maps, by using the microscopic Usadel approach[7,34] (Supplementary Information 3). Figure 4a shows the computed map of the local density of states at the Fermi energy for a junction similar to J1. The map demonstrates the suppression of the proximity gap inside Josephson vortex cores[7]. This suppression is further detailed in Fig. 4b, where we show the local density of states as a function of

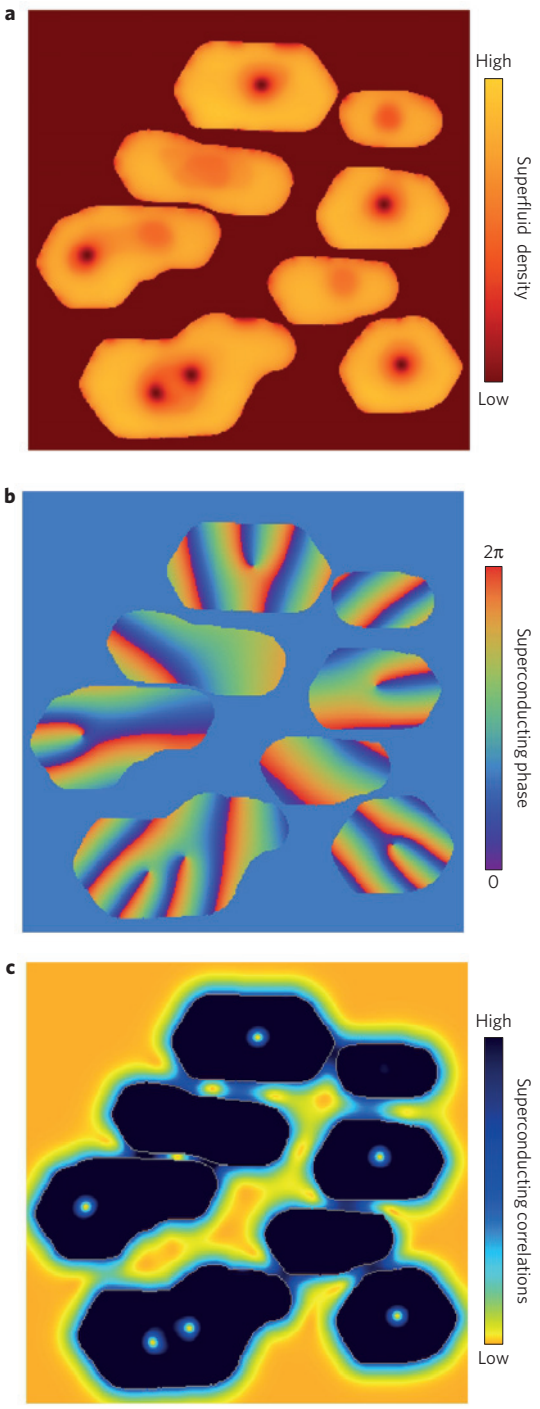

Figure 3 | Simulation of Josephson vortex maps. a, 1,000 nm × 1,000 nm colour-coded spatial distribution of the Cooper-pair density in the studied sample at 60 mT, calculated in the framework of the Ginzburg–Landau approach (see Supplementary Information). The superconducting and normal areas are yellow and brown, respectively. The proximity effect between nano-islands is neglected. Note the match with the experimentally observed Abrikosov vortex positions in Fig. 1c. **b**, Colour-coded phase portrait $\varphi_{GL}(\mathbf{r})$ corresponding to the situation in **a** and calculated in the symmetric gauge $\mathbf{A}(\mathbf{r}) = (1/2)\mathbf{B} \times \mathbf{r}$, with the origin chosen in the image centre. **c**, Correlation map at 60 mT, numerically generated using the maps in **a** and **b** together with the self-consistent gauge-invariant model developed here (see Supplementary Information 2 and explanations in the text). Note the detailed agreement with the experimental result shown in Fig. 1c.

energy at various distances from the centre of a vortex. Using these results we generated the corresponding tunnelling conductance spectra (Fig. 4c). In this calculation the Altshuler–Aronov zero-bias effect was taken into account[23]. As one can see, the Usadel approach reproduces qualitatively the observed vanishing of the proximity gap in Fig. 1e,f.

In the present experimental study, the gauge-invariant phase difference that generates Josephson vortices was created with the help of an applied magnetic field. Equivalently, the gauge-invariant phase differences may be generated by edge supercurrents circulating in S-electrodes. Indeed, in zero magnetic field, taking the gauge $\mathbf{A} = 0$, we get a simple expression relating the current and phase, $\mathbf{J} \approx J_c(\xi/\pi)\nabla\varphi$, where ξ is the effective coherence length, and J_c is the critical current in the electrode, $|\nabla\varphi| \leq (\pi/\xi)$. Therefore, if the superconducting electrodes of the junction carry oppositely directed currents along the electrode edge, a gauge-invariant phase difference appears across the junction. It evolves with the lateral position r inside the junction as $\varphi^*(r) \approx 2\pi(J/J_c)(r/\xi)$, leading to the formation of a Josephson vortex. To confirm this idea, we carried out calculations of the local density of states in SNS junctions where currents flow inside S-leads along the junction edges with no applied magnetic field (Supplementary Information 3). We show in Fig. 4d a typical result for a junction similar to J1, where we have assumed that opposite currents circulate along both interface edges. As one can see, there appear Josephson vortices with normal cores, very similar to those induced magnetically (see Fig. 4a). In this case, the density and size of generated Josephson vortices is simply proportional to the intensity of circulating edge currents. Moreover, vortex generation may also be achieved if only one superconducting lead carries a supercurrent, as we demonstrate in Fig. 4e. By tuning intensities of supercurrents in leads one may pin vortices at one or other edge. In a SNS device, such as the one sketched in Fig. 4f, it should be possible to create Josephson vortices by simply applying currents through superconducting leads. Such a method would open new pathways for generation and control of quantum objects by purely electrical means, without the need of any externally applied magnetic field.

Methods

The 7×7 reconstructed n-Si(111) ($n \approx 10^{19}$ cm^{-3}) was prepared by direct current heating to 1,200 °C, followed by annealing procedure between 900 and 500 °C. Subsequently, a few atomic layers of Pb were evaporated on the Si(111)-7×7 kept at room temperature, using an electron beam evaporator calibrated with a quartz micro-balance. The resulting flat-top (111)-oriented single nanocrystals of Pb are interconnected via a disordered atomic wetting layer of Pb (refs 23–28). During sample preparation the pressure did not exceed $P = 3 \times 10^{-10}$ mbar. The sample structure was controlled in both real and reciprocal space by scanning tunnelling microscopy and low-energy electron diffraction.

The scanning tunnelling spectroscopy measurements were performed *in situ* with a homemade apparatus, at a base temperature of 320 mK and in a ultrahigh vacuum with $P < 3 \times 10^{-11}$ mbar; the electron temperature was estimated to be 390 mK. Mechanically sharpened Pt/Ir tips were used. The bias voltage was applied to the sample with respect to the tip. Typical set-point parameters for spectroscopy are 150 pA at $V = -5$ mV. The tunnelling conductance curves $dI(V)/dV$ were numerically derived from raw $I(V)$ experimental data. Each conductance map is extracted from a set of data consisting of spectroscopic $I(V)$ curves measured at each point of a 512×512 grid, acquired simultaneously with the topographic image. The magnetic field was applied perpendicular to the sample surface.

The frameworks for the theoretical simulations in this paper are the phenomenological Ginzburg–Landau (GL) theory[4] and the microscopic Usadel approach[7,34]. The GL simulations were implemented on a Cartesian grid for the exact geometry of the islands and expected electron mean-free path in the samples (Supplementary Information 1), using STM mapping from the experiment, with a grid spacing of 1 nm. The equations were solved self-consistently in three dimensions and contain higher-order derivatives; for this demanding computation we have used GPU parallel computing. The description of the local density of states and tunnelling spectra of the SNS junctions was carried out using the Usadel approach, as explained in detail in the Supplementary Information 3.

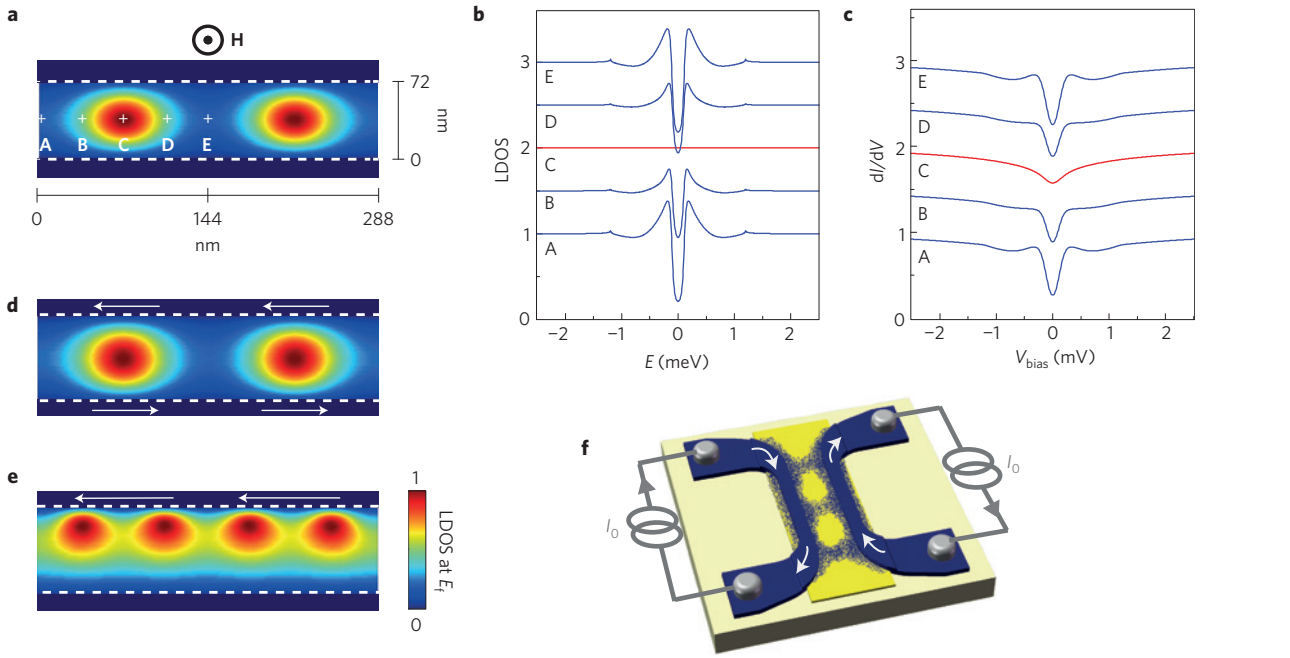

Figure 4 | Josephson vortex core: density of states and principle of generation by edge currents. a, Calculated spatial map of the density of states at the Fermi energy using the Usadel approach for a SNS junction similar to J1 (inter-electrode spacing 72 nm, as delimited by dashed lines, and length 288 nm) for a magnetic field of 200 mT. Notice the appearance of two Josephson vortices. **b**, Local density of states (LDOS) as a function of energy at the locations indicated in **a**. **c**, Conductance spectra calculated with the results for the density of states of **b** at 400 mK. **d**, Spatial map of the density of states at the Fermi energy computed using the Usadel approach showing Josephson vortices in SNS junction as in **a**, but generated solely by opposite edge currents circulating in superconducting electrodes. The currents are represented by white arrows. **e**, Same as in **d**, but for a junction where the edge current is present only in one lead. The vortices have asymmetric cores. A higher current density generates a denser Josephson vortex chain. **f**, Sketch of a minimal device allowing the all-electric generation and manipulation of Josephson vortices. It contains two superconducting electrodes (the narrow strips shown in blue), non-superconducting metal between (yellow), linking the two electrodes by the proximity effect. The junction length should be $W > 2\xi$ to accept one or more Josephson vortices (two Josephson vortices are shown). At least one of the two superconducting electrodes should carry an electric current (see text).

Received 15 April 2014; accepted 5 January 2015; published online 23 February 2015

References

1. De Gennes, P. G. Boundary effects in superconductors. *Rev. Mod. Phys.* **36,** 225–237 (1964).
2. Josephson, B. D. Possible new effects in superconductive tunnelling. *Phys. Lett.* **1,** 251–253 (1962).
3. Rowell, J. M. Magnetic field dependence of the Josephson tunnel current. *Phys. Rev. Lett.* **11,** 200–202 (1963).
4. Tinkham, M. *Introduction to Superconductivity* (McGraw Hill, 1996).
5. Ulrich Welp, U., Kadowaki, K. & Kleiner, R. Superconducting emitters of THz radiation. *Nature Photon.* **7,** 702–710 (2013).
6. Devoret, M. & Schoelkopf, R. Superconducting circuits for quantum information: An outlook. *Science* **339,** 1169–1174 (2013).
7. Cuevas, J. C. & Bergeret, F. S. Magnetic interference patterns and vortices in diffusive SNS junctions. *Phys. Rev. Lett.* **99,** 217002 (2007).
8. Andreev, A. F. Electron spectrum of the intermediate state of superconductors. *Zh. Eksp. Teor. Fiz.* **49,** 655–660 (1965) ; *Sov. Phys. JETP* **22**, 455–458 (1966).
9. Barone, A. & Paterno, G. *Physics and Applications of the Josephson Effect* (Wiley, 1982).
10. Heersche, H. B., Jarrillo-Herrero, P., Oostinga, O. O., Vandersypen, L. M. K. & Morpurgo, A. F. Bipolar supercurrent in graphene. *Nature* **446,** 56–59 (2007).
11. Veldhorst, M. *et al.* Josephson supercurrent through a topological insulator surface state. *Nature Mater.* **11,** 417–421 (2012).
12. Williams, J. R. *et al.* Unconventional Josephson effect in hybrid superconductor–topological insulator devices. *Phys. Rev. Lett.* **109,** 056803 (2012).
13. Abrikosov, A. A. On the magnetic properties of superconductors of the second group. *Sov. Phys. JETP* **5,** 1174–1182 (1957).
14. Maggio-Aprile, I. *et al.* Critical currents approaching the depairing limit at a twin boundary in $YBa_2Cu_3O_{7-\delta}$. *Nature* **390,** 487–490 (1997).
15. Song, C-L. *et al.* Suppression of superconductivity by twin boundaries in FeSe. *Phys. Rev. Lett.* **109,** 137004 (2012).
16. Brun, C. *et al.* Remarkable effects of disorder on superconductivity of single atomic layers of lead on silicon. *Nature Phys.* **10,** 444–450 (2014).
17. Tsuei, C. C. & Kirtley, J. R. Pairing symmetry in cuprate superconductors. *Rev. Mod. Phys.* **72,** 969–1016 (2000).
18. Blatter, G. & Geshkenbein, V. B. *The Physics of Superconductors* Vol. 1 (eds Bennemannand, K. H. & Kettersonet, J. B.) Ch. 10, 896–897 (Springer-Verlag, 2003).
19. Gurevich, A. Nonlocal Josephson electrodynamics and pinning in superconductors. *Phys. Rev. B* **46,** 3187(R) (1992).
20. Kogan, V. G. *et al.* Josephson junction in a thin film. *Phys. Rev. B* **63,** 144501 (2001).
21. Hess, H. F., Robinson, R. B., Dynes, R. C., Valles, J. M. & Waszczak, J. V. Scanning-tunneling-microscope observation of the Abrikosov flux lattice and the density of states near and inside a fluxoid. *Phys. Rev. Lett.* **62,** 214–216 (1989).
22. Zhang, T. *et al.* Superconductivity in one-atomic-layer metal films grown on Si(111). *Nature Phys.* **6,** 104–108 (2010).
23. Serrier-Garcia, L. *et al.* Scanning tunneling spectroscopy study of the proximity effect in a disordered two-dimensional metal. *Phys. Rev. Lett.* **110,** 157003 (2013).
24. Eom, D., Qin, S., Chou, M-Y. & Shih, C. K. Persistent superconductivity in ultrathin Pb films: A scanning tunneling spectroscopy study. *Phys. Rev. Lett.* **96,** 027005 (2006).
25. Nishio, T. *et al.* Superconducting Pb island nanostructures studied by scanning tunneling microscopy and spectroscopy. *Phys. Rev. Lett.* **101,** 167001 (2008).
26. Cren, T., Fokin, D., Debontridder, F., Dubost, F. & Roditchev, D. Ultimate vortex confinement studied by scanning tunneling spectroscopy. *Phys. Rev. Lett.* **102,** 127005 (2009).
27. Brun, C. *et al.* Reduction of the superconducting gap of ultrathin Pb islands grown on Si(111). *Phys. Rev. Lett.* **102,** 207002 (2009).
28. Cren, T., Serrier-Garcia, L., Debontridder, F. & Roditchev, D. Vortex fusion and giant vortex states in confined superconducting condensates. *Phys. Rev. Lett.* **107,** 097202 (2011).
29. Altshuler, B. L. & Aronov, A. G. in *Electron–Electron Interactions in Disordered Systems* (eds Efros, A. L. & Pollak, M.) (Elsevier Science Publisher B. V., 1985).

30. Golubov, A. A. & Kupriyanov, M. Y. Theoretical investigation of Josephson tunnel junctions with spatially inhomogeneous superconducting electrodes. *J. Low Temp. Phys.* **70,** 83–130 (1988).
31. Belzig, W. *et al.* Local density of states in a dirty normal metal connected to a superconductor. *Phys. Rev. B* **54,** 9443–9448 (1996).
32. Kim, J. *et al.* Visualization of geometric influences on proximity effects in heterogeneous superconductor thin films. *Nature Phys.* **8,** 464–469 (2012).
33. Le Sueur, H., Joyez, P., Pothier, H., Urbina, C. & Esteve, D. Phase controlled superconducting proximity effect probed by tunneling spectroscopy. *Phys. Rev. Lett.* **100,** 197002 (2008).
34. Usadel, K. D. Generalized diffusion equation for superconducting alloys. *Phys. Rev. Lett.* **25,** 507–509 (1970).

Acknowledgements

T.C., C.B., F.D., V.S. and D.R. acknowledge financial support from the French ANR project ELECTROVORTEX and the French-Russian program PICS-CNRS/RAS. The authors also thank V. Cherkez for assistance during experiments and V. Vinokur (Argonne National Laboratory, Illinois USA) and A. Buzdin (University of Bordeaux 1, France) for stimulating discussions. J.C.C. acknowledges financial support from the Spanish MICINN (Contract No. FIS2011-28851-C1). V.H.L.B. acknowledges support from CNPq Brazil and productive discussions with Prof. A. Chaves (UFC, Brazil). M.V.M. acknowledges support from Research Foundation Flanders (FWO-Vlaanderen) and CAPES Brazil (PVE project BEX1392/11-5).

Author contributions

The experiments were conceived by D.R., T.C., C.B. and F.D. The experiments were performed by C.B., D.R., L.S-G., T.C., V.S. and F.D. Theoretical support was provided by J.C.C., V.H.L.B. and M.V.M. Superconducting correlation maps were calculated by T.C. The manuscript was written by D.R., J.C.C. and T.C. with comments and input from all authors.

Additional information

Supplementary information is available in the online version of the paper. Reprints and permissions information is available online at www.nature.com/reprints. Correspondence and requests for materials should be addressed to T.C.

Competing financial interests

The authors declare no competing financial interests.